Prahalad K. Rao
Department of Systems Science
and Industrial Engineering,
Binghamton University,
Binghamton, NY 13902-6000

Zhenyu Kong[1]
Grado Department of Industrial
and Systems Engineering,
Virginia Tech,
Blacksburg, VA 24061
e-mail: zkong@vt.edu

Chad E. Duty
Oak Ridge National Laboratory,
P.O. Box 2008,
Oak Ridge, TN 37831-6083;
Department of Mechanical, Aerospace and
Biomedical Engineering,
The University of Tennessee,
Knoxville, TN 37996-2210

Rachel J. Smith
Department of Biomedical Engineering,
University of California, Irvine,
Irvine, CA 92617

Vlastimil Kunc
Oak Ridge National Laboratory,
P.O. Box 2008,
Oak Ridge, TN 37831-6083

Lonnie J. Love
Oak Ridge National Laboratory,
P.O. Box 2008,
Oak Ridge, TN 37831-6083

Assessment of Dimensional Integrity and Spatial Defect Localization in Additive Manufacturing Using Spectral Graph Theory

The ability of additive manufacturing (AM) processes to produce components with virtually any geometry presents a unique challenge in terms of quantifying the dimensional quality of the part. In this paper, a novel spectral graph theory (SGT) approach is proposed for resolving the following critical quality assurance concern in the AM: how to quantify the relative deviation in dimensional integrity of complex AM components. Here, the SGT approach is demonstrated for classifying the dimensional integrity of standardized test components. The SGT-based topological invariant Fiedler number (λ_2) was calculated from 3D point cloud coordinate measurements and used to quantify the dimensional integrity of test components. The Fiedler number was found to differ significantly for parts originating from different AM processes (statistical significance p-value <1%). By comparison, prevalent dimensional integrity assessment techniques, such as traditional statistical quantifiers (e.g., mean and standard deviation) and examination of specific facets/landmarks failed to capture part-to-part variations, proved incapable of ranking the quality of test AM components in a consistent manner. In contrast, the SGT approach was able to consistently rank the quality of the AM components with a high degree of statistical confidence independent of sampling technique used. Consequently, from a practical standpoint, the SGT approach can be a powerful tool for assessing the dimensional integrity of the AM components, and thus encourage wider adoption of the AM capabilities. [DOI: 10.1115/1.4031574]

Keywords: additive manufacturing (AM), fused filament fabrication (FFF), dimensional integrity, geometric deviations, 3D point cloud data, defect localization, spectral graph theory, Fiedler number

1 Introduction

1.1 Objective and Motivation. The objective of this work is to quantify the relative deviation in dimensional integrity of components made using AM processes, and subsequently, rank/classify AM components in terms of their dimensional integrity. We propose a novel spectral graph theoretic (SGT) approach, which uses 3D point cloud data obtained from laser line scans of AM components to realize this objective. The SGT approach *compares* the dimensional integrity of AM parts. In other words, using the proposed SGT approach, the dimensional integrity of two or more AM parts can be ranked relative to each other; an absolute measurement, e.g., in terms of geometric dimensioning and tolerancing (GD&T) callouts, is not proffered.

AM processes can create components with complex facets, which are difficult, if not impossible, to craft using conventional subtractive and formative manufacturing techniques [1,2]. However, the lack of quantitative approaches for assessing dimensional integrity deters the use of AM components, despite several functional advantages, into mission critical assemblies [3]. It is therefore essential to overcome this limitation in order to realize the benefits offered by the AM [4,5]. This work aims to address the foregoing research gap in the context of dimensional integrity quantification in AM.

1.2 Research Challenges. The imperative need for novel quantitative approaches to assess dimensional integrity in AM is further motivated in terms of the experimental data from this research as depicted in Fig. 1. The laser scan probe 3D point cloud data of geometric deviations for three AM components produced at Oak Ridge National Laboratory (ORNL) (see also Sec. 3.1) are represented as flooded contour plots in Fig. 1. These components are standardized AM test artifacts proposed by NIST [6].

The three components in Fig. 1 are produced using a polymer extrusion AM process called fused filament fabrication (FFF)[1] [1]. They are made with two different materials, namely, acrylonitrile butadiene styrene (ABS) thermoplastic (Figs. 1(*a*) and 1(*b*)) and carbon fiber (CF) impregnated thermoplastic ABS composite (CF-ABS) (Fig. 1(*c*)), and varying process conditions on two separate build platforms [7]. The process conditions are described in further detail in Sec. 3.1.1. The objective of this study was to classify the components in Figs. 1(*a*)–1(*c*) based on their dimensional integrity using a rigorous quantitative approach. The desired output was a statistically relevant ranking of the components based

[1]Corresponding author.

Contributed by the Manufacturing Engineering Division of ASME for publication in the Journal of Manufacturing Science and Engineering. Manuscript received February 27, 2015; final manuscript received September 1, 2015; published online November 19, 2015. Assoc. Editor: Z. J. Pei.

The United States Government retains, and by accepting the article for publication, the publisher acknowledges that the United States Government retains, a nonexclusive, paid-up, irrevocable, worldwide license to publish or reproduce the published form of this work, or allow others to do so, for United States government purposes.

[1]Also often referred as Fused Deposition Modeling (FDM), a trademark of Stratasys, Inc.

Copyright © 2016 by ASME

Downloaded From: https://manufacturingscience.asmedigitalcollection.asme.org/ on 11/24/2015 Terms of Use: http://www.asme.org/about-asme/terms-of-use

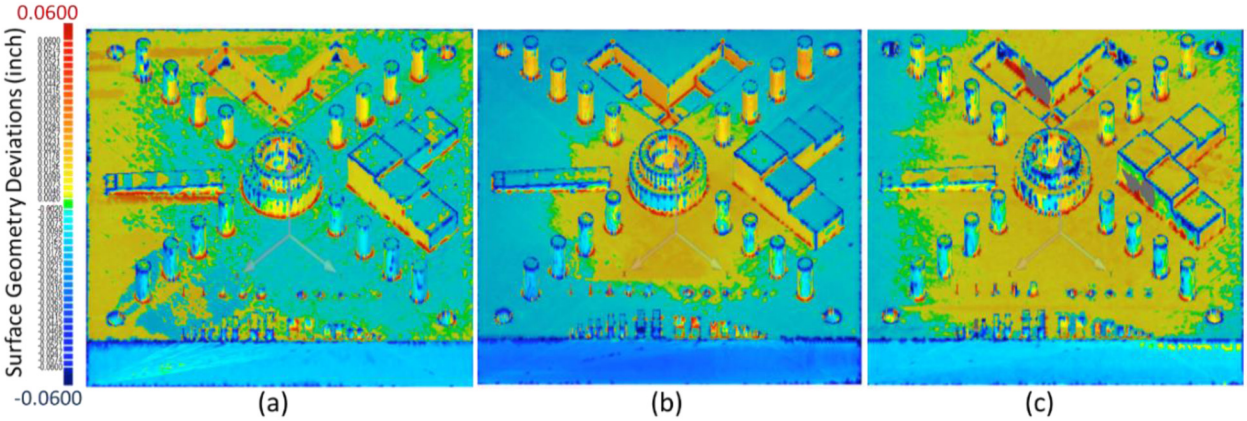

Fig. 1 Plots showing surface geometry deviations (inches) obtained from 3D point cloud data for three different AM samples (see Sec. 3.1 for further details). The AM samples shown here measure 100 mm × 100 mm × 8 mm (4 in. × 4 in. × 0.3 in.). (*a*) and (*b*) Components produced using ABS thermoplastic but different processing conditions (see Sec. 3.1, Table 1). (*c*) Component produced using CF impregnated thermoplastic composite (CF-ABS).

on the deviations of the measured dimensions from the original design specifications.

Visually prominent qualitative differences in dimensional integrity of the components can be discerned from their point cloud data as shown in Fig. 1. Closer examination of Fig. 1 reveals that the CF composite component in Fig. 1(*c*) is expected to most closely match the design specifications (i.e., have the best dimensional integrity), given that large areas of the part have almost zero deviation. The component in Fig. 1(*a*) seems to have the next best correlation to the design specifications. The component in Fig. 1(*b*) has perhaps the worst dimensional integrity given the predominance of areas with negative deviations. These observations corroborate our recent research findings at ORNL (see Ref. [7]) where it was demonstrated that CF-containing raw materials not only improve the mechanical performance of AM parts, but also significantly reduce geometric distortion during material deposition.

However, as demonstrated in Sec. 3.1.3, quantifying the differences in dimensional integrity of the components shown in Fig. 1 using statistical parameters, such as mean and standard deviation of 3D point cloud deviations, and conventional facet/landmark measurements was ineffective. It was not possible to detect a significant difference (p-value $< 10\%$) in dimensional integrity for the three components in Fig. 1 based on conventional statistical feature mining and facet examination techniques. This difficulty in quantifying geometric integrity of the AM components has also concerned other researchers (see, e.g., Refs. [8–14]).

1.3 Novelty and Significance. The intractability in characterizing the dimensional integrity of the AM parts using traditional descriptive statistical features and facet measurement techniques from 3D point cloud data, as illustrated in Fig. 1, and also further documented in Sec. 3.1.3, has motivated us to pursue an alternative approach. The main contribution of this work is in a novel SGT approach that captures the relative geometric deviation (i.e., difference or imprecision with respect to the CAD blueprint) in dimensional integrity of AM parts from 3D point cloud measurements with one effective quantifier derived from SGT, namely, the Fiedler number (λ_2) [15,16]. The effectiveness of the Fiedler number to overcome much of the limitations with traditional statistical feature mining and facet examination is demonstrated in this work using experimentally acquired, as well as computer generated 3D point cloud data. The proposed SGT-based approach for quantification of AM dimensional integrity is practically advantageous in the following aspects:

(1) The approach uses 3D point cloud data as an input, which is a noncontact measurement technique unlike using a coordinate measuring machine (CMM). Additionally, the approach uses an analysis technique that is not scale limited. Consequently, the measurement and analysis process is quicker and flexible as coordinates and facets are not required to be predefined as in the CMM.
(2) The dimensional integrity of free-form surfaces is tracked on the basis of one scalar quantifier, namely, the Fiedler number (λ_2).
(3) Apart from classifying the overall dimensional integrity, the Fiedler number (λ_2) can be used to monitor the status of specific spatial locations on the component. This can facilitate redesign of troublesome component features or readjustment of process conditions in the future.

We note that the Fiedler number (λ_2) is akin to a comparative gage, it can classify the relative quality of the AM parts. However, the main shortcoming of the proposed approach is that the Fiedler number (λ_2) has not been correlated with GD&T measurements. Thus, we cannot infer, at this juncture, the GD&T aspects of an AM component given the Fiedler number (λ_2). We reiterate that the proposed SGT approach is a ranking method for assessing the dimensional integrity of AM components, and as such is not intended to tender an absolute measurement in terms of GD&T. Our future research objective is to quantify the Fiedler number (λ_2) trends with specific GD&T measurements.

The rest of this paper is structured as follows: previous research in metrology using 3D point cloud data is briefly reviewed in Sec. 2; the research methodology and development of the SGT approach for quantifying dimensional integrity of the AM parts is described in Sec. 3; followed by application of the SGT approach to experimental AM point cloud data and further verification using artificially generated components in Sec. 4; and finally, concluding remarks are summarized in Sec. 5.

2 A Brief Review of Related Research

Dimensional integrity studies in the AM have thus far largely relied on either: (i) categorical/visual evaluations [17]; (ii) measurement of salient characteristics of specific facets/landmarks on the component [18]; or (iii) GD&T measurements using CMM [19]. These approaches provide only a partial perspective of the overall dimensional integrity of the component, and are noted to be fraught with limitations stemming from their subjective nature and inability to distinguish subtle geometrical differences [20]. Furthermore, conventional GD&T and facet examination techniques are primarily intended for regular Euclidean features, and are

Downloaded From: https://manufacturingscience.asmedigitalcollection.asme.org/ on 11/24/2015 Terms of Use: http://www.asme.org/about-asme/terms-of-use

therefore not amenable for assessment of AM parts with complex free-form geometries [4,20]. Hence, quantification of dimensional integrity of AM parts remains an imposing challenge [3,8,21]. An alternative approach is to maintain the dimensional integrity of AM components by avoiding errors during the build process. In this context, adaptive slicing techniques [22,23], and feedback control approaches have been recently suggested [24,25].

Metrology of free-form geometry parts, particularly using 3D point cloud data, has recently garnered substantial research attention, primarily driven by the emergence of AM techniques. A number of review articles have been published recently in the area of free-form dimensional metrology using noncontact techniques, such as laser scanning and computed tomography (CT) [4,26–28]. Point cloud data have previously been used in dimensional metrology of automotive parts, buildings, biomedical prosthetics, geospatial applications, etc. [4,28,29]. For instance, Raja et al. [30] evaluated six different AM methods, viz., stereolithography, selective laser sintering, laser melting, 3D plotting with thermoform material, material jetting, and fused deposition modeling (FDM) for production of two aerospace components. The AM parts were scanned with a laser-based profile scanner, and subsequently, the component geometry was reconstructed from the acquired 3D point cloud data. The parts were quantified based upon morphological aspects, such as surface finish, geometric accuracy, and functional fitness using the reconstructed geometry. The following inferences pertinent to our work can be drawn from the results reported by Raja et al. [30]:

- Surface finish and dimensional integrity of the AM parts were independent. For instance, while the multimaterial jetting process affords good surface finish, the produced components had one of the worst geometric accuracies. Thus, a quality variable, such as surface finish, should not be used as surrogate indicator for dimensional integrity.
- AM components showed the presence of location dependent anomalies, i.e., specific areas of the part, e.g., edges, were not accurately reproduced, whereas the other areas were satisfactory. Hence, it is important to not only quantify the overall dimensional integrity but also localize dimensional variations contingent on the spatial geometry of the part. In other words, it is relevant to indicate the faulty locations on the component.
- Difficulty in quantitatively gauging the dimensional integrity of AM components; indeed, the majority of results reported by Raja et al. are based on qualitative criteria.

There is a bourgeoning need for the use of point cloud data as an analytical tool to assess geometric deviations in AM, and subsequently, relating the result to the process for diagnostic purposes. The SGT approach forwarded in this work attempts to bridge the foregoing gap.

3 Research Methodology

Figure 2 distills the three main parts of the proposed research work, namely:

(1) **Experimental procedure (Sec. 3.1):** The NIST standard AM test artifact was used as the geometric reference for this investigation. Test components were manufactured at ORNL using three different combinations of deposition technique and materials [6]. The three components are labeled as ABS chamber, ABS platform, and CF-ABS platform. Further details of their manufacture are provided in Sec. 3.1.1.
Subsequently, in Sec. 3.1.2, the component geometry was assessed with a linear laser scanning probe (FaroArm Platinum) and stored as a 3D point cloud. The test component coordinate measurements ($\mathcal{T}^{\mathrm{N}\times\mathrm{d}}$) were compared to the corresponding design reference coordinates ($\mathcal{R}^{N\times d}$) from the.stl computer-aided design (CAD) file; where N is the number of measurement points and d is the dimension of the coordinate axes (Cartesian). In our case, N is ~500,000 and $d = 3$. The difference between the test component and design reference coordinates, $\mathcal{T} - \mathcal{R} = \mathcal{X}^{\mathrm{N}\times\mathrm{d}}$, is termed the point cloud *deviation matrix*. Our aim is to classify the quality of AM test parts based on their dimensional integrity, as measured in terms of the 3D point cloud coordinate deviations contained in $\mathcal{X}$.

(2) **SGT approach for quantifying dimensional integrity of AM components (Sec. 3.2):** A SGT approach is presented for monitoring the dimensional integrity of AM test components based on the 3D point cloud deviation matrix $\mathcal{X}$ obtained in Sec. 3.1. The main outcome of Sec. 3.2 is the representation of the deviation matrix $\mathcal{X}$ as a network graph G (Sec. 3.2.1), and subsequent quantification of the topology of the network G using an SGT invariant, namely, Fiedler number (λ_2) in 3.2.2. The graph theoretic topological invariant Fiedler number (λ_2) is used in this work for quantifying the dimensional integrity of AM test parts. Furthermore, in order to make the computation of the Fiedler number (λ_2) practically tenable, two different sampling methods are proposed to the SGT approach in Sec. 3.2.3.

(3) **Application of SGT to AM parts and verification with artificially generated surfaces (Sec. 4):** The above two-step SGT approach is applied to AM test parts (Sec. 4.1), and subsequently verified with artificially generated test parts (Sec. 4.2).

3.1 Experimental Procedure. The test artifact printed for this study was designed and developed by Moylan et al. [6] at NIST. This so-called NIST test artifact has become the industry standard for comparison among various AM processes and material combinations. Figure 3 illustrates the various part features, including cylinders, holes, ramps, fine features, edges, staircases, pins, holes, and flat surfaces. The part measures ~100 mm × 100 mm × 8 mm (4 in. × 4 in. × 0.3 in.). Each feature is designed to evaluate a specific capability of the AM process based on the limits of dimensional accuracy [6].

3.1.1 Manufacture of Test Components. The components examined in this study were manufactured using a polymer-based material extrusion AM process, called FFF [1]. The process is oftentimes referred as FDM™, which is a protected trademark of Stratasys, Inc. In FFF, typically, a thermoplastic material is heated past the glass transition temperature and extruded through a nozzle in a controlled manner [1]. The three component types studied in this work are designated by the type of material used for deposition and the primary heat source for controlling thermal distortion during manufacture. These were shown previously in Sec. 1, Fig. 1. For instance, the first component (Fig. 1(*a*) is made with ABS plastic in a machine having a thermally controlled build chamber, and is thus labeled as *ABS chamber*. Table 1 summarizes the conditions for the manufacture of the three different types of AM components, namely, ABS chamber, ABS platform, and CF-ABS platform.

3.1.2 Description of Measurement Procedure and Data. The three samples were scanned with a FaroArm Platinum linear scanning laser probe to generate a three-dimensional point cloud. A representative sample scan consisting of ~500,000 data points is shown in Fig. 3. The laser scanner records reflected light from the surface of a component as a point in 3D space, with a maximum volumetric deviation of ±43 μm. The point cloud for each part was then imported into a commercial software package (GEOMAGIC by 3DSystems) for analysis. Standard functions within the software are used to remove outlier points and disconnected components. The error-corrected 3D point cloud data is subsequently converted to a polygon mesh for comparison against the reference CAD model in order to assess the geometric accuracy of the component.

The polygon mesh and CAD model were numerically compared by measuring the normal distance from a point on the mesh to the closest surface of the CAD model. The geometric 3D point cloud

Downloaded From: https://manufacturingscience.asmedigitalcollection.asme.org/ on 11/24/2015 Terms of Use: http://www.asme.org/about-asme/terms-of-use

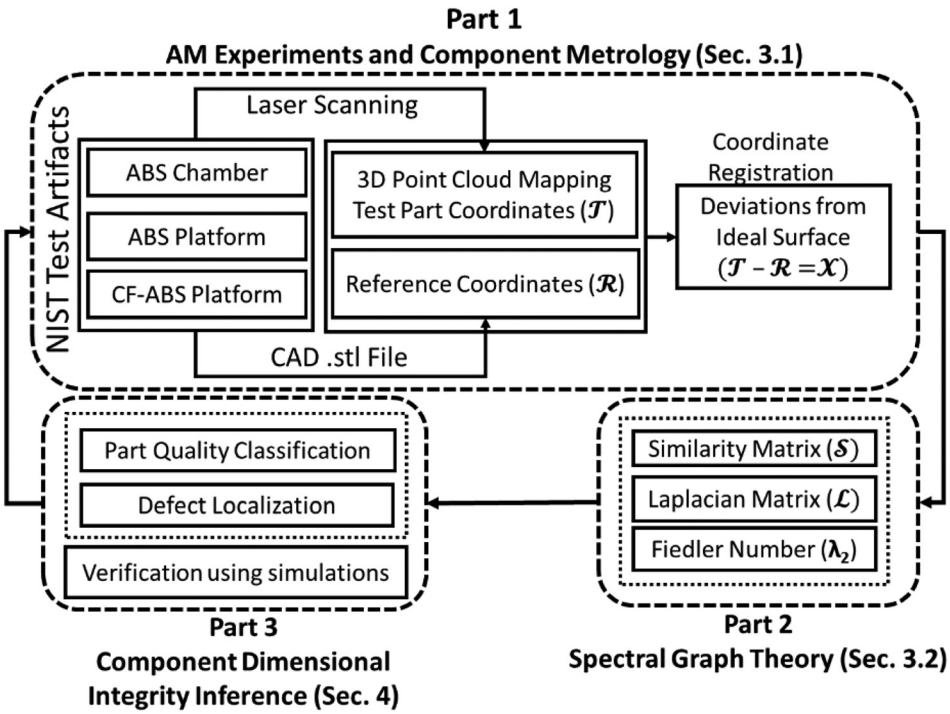

Fig. 2 Summary of the research methodology

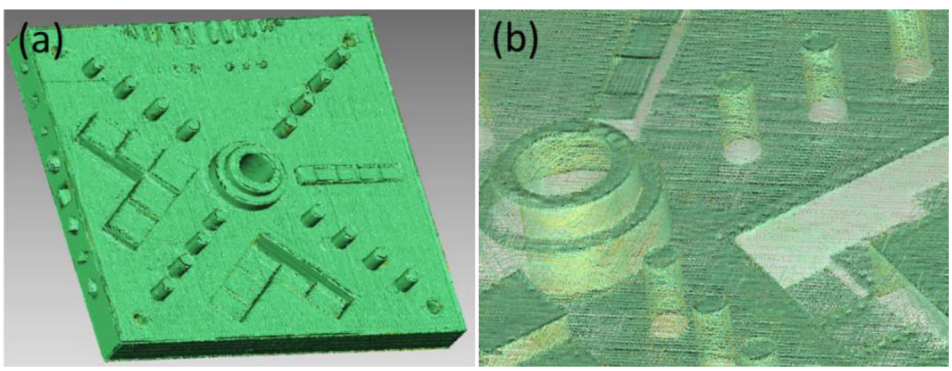

Fig. 3 (*a*) 3D Point cloud of NIST part (100 mm × 100 mm × 8 mm; 4 in. × 4 in. × 0.3 in.) obtained using the FaroArm laser scanning probe. (*b*) Zoomed in section showing fine features (4 × zoom).

Table 1 Material and processing conditions for the three types of test components studied in this work

	Component type		
Build characteristics ↓	ABS chamber Fig. 1(*a*)	ABS platform Fig. 1(*b*)	CF-ABS platform Fig. 1(*c*)
Material	ABS*plus*-P430 (Stratasys)	Generic 1.75 mm ABS filament (makergeek.com)	Tailored CF-ABS. See Ref. [7]
Machine	Stratasys uPrint SE Plus FDM™ machine	Solidoodle 3 desktop FFF machine	Modified Solidoodle 3 desktop FFF machine
Thermal distortion control	Heated build chamber (77 °C)	Heated build platform (85 °C)	Heated build platform (85 °C)
Extrusion Temperature	310 °C	205 °C	215 °C
Layer height	0.330 mm	0.20 mm	0.40 mm
Toolpath and direction	Two perimeter contours, 45 deg sparse raster fill. Slicing algorithm was similar for each system.		

data thus obtained is structured as a matrix consisting of nine columns, which are: (i–iii) Cartesian coordinates of the reference point on the CAD model $\mathcal{R}^{N\times 3} = \{X\text{ref}, Y\text{ref}, Z\text{ref}\}$; (iv–vi) the coordinates of the reference point from the measured polygon mesh $\mathcal{T}^{N\times 3} = \{X\text{mesh}, Y\text{mesh}, Z\text{mesh}\}$; and (vii–ix) the deviation $\mathcal{T} - \mathcal{R} = \mathcal{X}^{N\times 3}$ between the measured and CAD coordinate. Consequently, the point cloud deviations contain information of various aspects of the part, e.g., profile, line, and GD&T (but not

Downloaded From: https://manufacturingscience.asmedigitalcollection.asme.org/ on 11/24/2015 Terms of Use: http://www.asme.org/about-asme/terms-of-use

the finer surface texture, because of the resolution of the laser scanner, viz., ± 43 μm).

The deviations from the reference geometry can be visualized as flooded contour plots as shown previously in Fig. 1. Although the flooded contours of the geometric variations are an intuitive way to visualize the integrity of the part, quantification of these variations is challenging. In Sec. 3.1.3, the limitations of conventional statistical analysis and facet examination techniques in quantifying geometric integrity of complex AM parts from 3D point cloud data measurements is demonstrated.

3.1.3 Selection of Benchmark Methods for Evaluation of AM Test Components. This section demonstrates that statistical feature mining of 3D point cloud data and facet examination approaches are not effective for assessment of the AM parts with complex free-form geometries [4,20]. These will serve as benchmarks to compare against the SGT approach proposed in this work. As noted previously in the literature review (Sec. 2), these are the most popular approaches currently used for dimensional integrity monitoring from 3D point cloud data [31].

Benchmark method 1—Analyzing basic statistical moments of 3D point cloud deviations. An intuitive method for analyzing the 3D point data would be to estimate the statistical moments of the point cloud data, e.g., mean and standard deviation. For instance, the mean absolute deviation in all Cartesian directions (x, y, z) is compared to the three test parts in Fig. 4(*a*) (for varying sample sizes). From Fig. 4(*a*), it becomes apparent that the ABS chamber and CF-ABS platform samples have statistically less geometric deviation than the ABS platform sample—a trend that becomes more obvious as the sample size increases.

However, if deviations only in the z-direction are evaluated, as in Fig. 4(*b*), both of the platform-heated samples (ABS platform and CF-ABS platform) appear to be much less accurate than the ABS chamber sample. Thus, it is possible to arrive at contradictory conclusions when applying similar statistical moments to different portions of the overall 3D point cloud data. Contradictory results were obtained using other descriptive statistics, such as standard deviation, skewness, and kurtosis. Therefore, from the comparison of Figs. 4(*a*) and 4(*b*), statistical feature mining of 3D point cloud data could ineffectual and fraught with ambiguity for dimensional integrity classification.

Contemporary distribution fitting approaches, such as mixture Gaussian models, and supervised learning algorithms, e.g., neural networks will most probably be able to overcome these limitations, and provide an unambiguous classification of an AM dimensional integrity from 3D point cloud data. However, these concepts are difficult to translate to an operational environment, in terms of one simple quantifier. In contrast, the SGT approach proposed in this work characterizes the relative dimensional integrity with one quantifier, namely, the Fiedler number. We will corroborate this assertion in Sec. 4 in the context of the AM part quality quantification.

Benchmark method 2—Examination of specific component facets/landmarks. The geometric deviations of specific component facets/landmarks within corresponding planar cross sections of the part were also analyzed. For this purpose, as shown in Fig. 5(*a*), individual line scans were used to isolate geometric deviations for specific facets. These are: (i) *edge distortions* as indicated by red lines in Fig. 5(*a*); (ii) *fine features* demarcated by green lines; and (iii) *flatness* of the surface planes represented with blue lines. A positive deviation indicates the point lies outside the CAD model, whereas a negative deviation indicates the point lies in the interior of the model. The results are summarized in Table 2 and plotted for comparison in Fig. 5(*b*). The following general trends may be observed:

(1) The magnitude of geometric deviations (positive and negative deviations) appears to be roughly equal for the ABS chamber and CF-ABS platform samples.
(2) The ABS platform sample has about 30% higher deviation on average than the other two components, highlighting the positive effect of the heated chamber on geometric structures for the ABS materials.
(3) The edge and flatness facets show that the ABS chamber sample has less overall deviation than the other two samples, and less negative deviations in each case.
(4) Comparing the magnitude of the deviations between the ABS platform and the CF-ABS platform indicates that the reinforced CF filament material holds geometric tolerance ~30% better than the ABS material on the same build system.
(5) Although it is possible to use facet examination to make some general observations, it must be noted that the standard deviation for the data in Table 2 is ~180 μm. Therefore, the foregoing observations are not statistically tenable. We found that the facet measurements for the three samples were statistically indistinguishable (p-val. $\gg$ 10%).

These observations show that the quantification of part quality for a complex geometry, which has been a long-standing and inherent problem in AM, cannot be resolved using traditional statistical feature mining and facet examination techniques. A different method for assessing part quality is therefore needed to address qualification of complex AM components in critical applications.

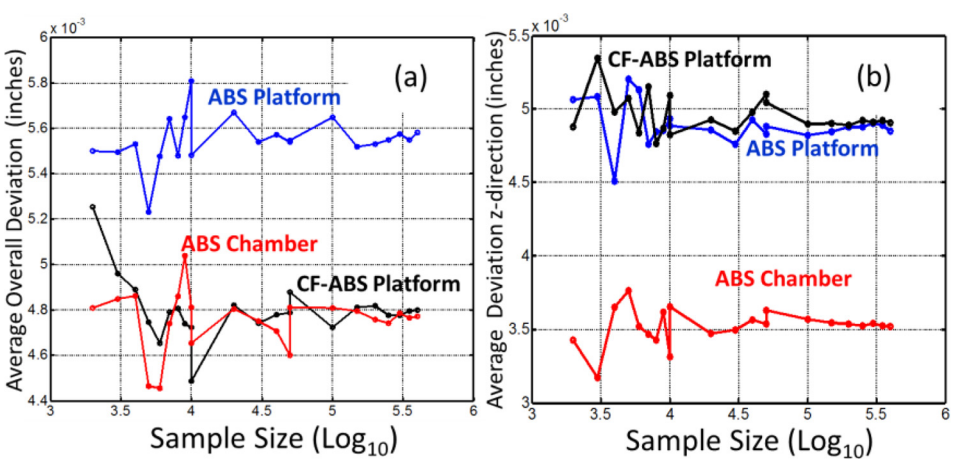

Fig. 4 (*a*) Average deviation of point cloud data in *x*, *y*, and *z* directions (overall deviation). (*b*) Average deviation in the vertical (*z*) direction. The ambiguity of statistical feature mining approaches for quantifying dimensional integrity is observed in comparison of (*a*) and (*b*).

Downloaded From: https://manufacturingscience.asmedigitalcollection.asme.org/ on 11/24/2015 Terms of Use: http://www.asme.org/about-asme/terms-of-use

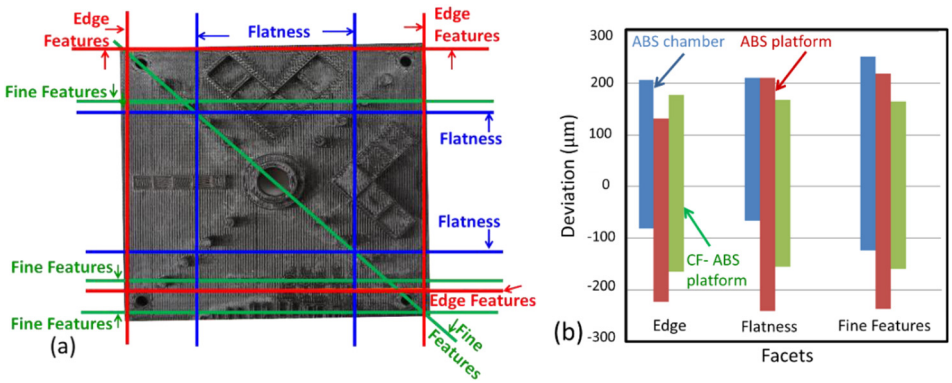

Fig. 5 (*a*) Line scan locations for analysis of specific facets. (*b*) Feature deviations for facet-specific line scans.

The SGT approach developed in this work, and discussed herewith, presents an opportunity for fulfilling this need.

3.2 Graph Theoretic Approach for Component Dimensional Integrity Monitoring in AM. In this section, the procedure for converting a 3D point cloud dataset into a network graph is explained (Sec. 3.2.1). Thereafter, the network graph is quantified using topological invariants (Sec. 3.2.2). The section ends by describing different methods for adapting the SGT approach in a practical scenario (Sec. 3.2.3).

3.2.1 Mapping the 3D Point Cloud ($\mathcal{X}$) as a Network Graph (G). The objective of this section is to represent a sequence $\mathcal{X}$ of 3D point cloud data as a network graph G, i.e., achieve the mapping $\mathcal{X} \mapsto G$. Consider a sequence, $\mathcal{X} = x_1, x_2 \cdots x_{\mathrm{N}}$, where each x_i is a $1 \times \mathrm{d}$ vector. Essentially, $\mathcal{X}$ can be recast in matrix form with its rows indexed by x as follows:

$$\mathcal{X} = \begin{bmatrix} x_1^1 & \cdots & x_1^{\mathrm{d}} \\ \vdots & \ddots & \vdots \\ x_{\mathrm{N}}^1 & \cdots & x_{\mathrm{N}}^{\mathrm{d}} \end{bmatrix} \tag{1}$$

From a 3D point cloud perspective, in Eq. (1) each row of $\mathcal{X}$ corresponds to a coordinate location along the Cartesian plane $\{x, y, z\}$, i.e., $d = 3$. At this juncture, no sampling conditions have been imposed on $\mathcal{X}$ and it is assumed that $\mathcal{X}$ is an arbitrary sample of size N. Different sampling conditions will be progressively imposed on $\mathcal{X}$ in Sec. 3.2.3.

Table 2 Geometric deviations for line scans for different components (all units in micrometers (μm))

ABS chamber				
Deviations →		Positive deviation	Negative deviation	Difference
Facets	Edge	206	−81	287
	Flatness	211	−66	277
	Fine features	251	−125	376
ABS platform				
Deviations →		Positive deviation	Negative deviation	Difference
Facets	Edge	132	−224	356
	Flatness	211	−241	452
	Fine features	218	−236	454
CF-ABS platform				
Deviations →		Positive deviation	Negative deviation	Difference
Facets	Edge	178	−165	343
	Flatness	168	−155	323
	Fine features	165	−160	325

As a further note, in this work, unless otherwise stated, the matrix $\mathcal{X}$ contains deviations of test parts from the ideal designed dimensions. The individual deviations x_i are obtained by subtracting the reference geometry $\mathcal{R}$ of the component from the originating CAD.stl file from the geometry $\mathcal{T}$ of test part (measured using a laser scanner), $\mathcal{T} - \mathcal{R} = \mathcal{X}^{N\times 3}$. The coordinates of the test part are aligned with the.stl file using coordinate registration software (Geomagic by 3D Systems). For the N rows of $\mathcal{X}$, pairwise comparison metrics ω_{ij} are computed using a kernel function Ω. In this work, the following radial basis kernel is used. The constitutive equations of our approach are as follows:

$$\omega_{ij} = \Omega(x_i, x_j) = e^{-\left(\frac{\|x_i - x_j\|^2}{\sigma^2 \varepsilon}\right)} \forall\ i,j \in \{1 \cdots \mathrm{N}\}. \tag{2a}$$

$$\mathcal{E}^{\mathrm{N}\times\mathrm{N}} = \|x_i - x_j\|^2 \tag{2b}$$

$$\Theta(\omega_{ij}) = w_{ij} = \begin{cases} 1, & \omega_{ij} \le r \\ 0. & \omega_{ij} > r \end{cases} \tag{3a}$$

$$\mathbf{S}^{\mathrm{N}\times\mathrm{N}} = [w_{ij}] \tag{3b}$$

x_i is essentially a row from the matrix $\mathcal{X}$; ω_{ij} is a pairwise radial basis distances between two rows i and j; $r = (\sum_{i=1}^{N} \sum_{j=1}^{N} \omega_{ij}/N^2)$; and $\sigma^2{}_{\mathcal{E}}$ is the overall statistical variation of the Euclidean distance matrix $\mathcal{E}$. Equations (2) and (3) are the keystones of the SGT method. Equations (2) and (3) are particularly important because they convert a 3D point cloud data into an *unweighted undirected* graph.

3.2.2 Quantification of Graph Network Topology. Once the point cloud data $\mathcal{X}$ is represented as a graph G, relevant topological information is extracted from G, which is subsequently used for quantifying $\mathcal{X}$. For this purpose, the *degree* d_i of a node i is computed, which is a count of the number of edges that are incident upon the node, and the diagonal *degree matrix* $\mathcal{D}$ structured from d_i is obtained as follows:

$$d_i = \sum_{j=1}^{j=\mathrm{N}} w_{ij} \ \forall\ i,j \in \{1 \cdots \mathrm{N}\} \tag{4}$$

$$\mathcal{D}^{\mathrm{N}\times\mathrm{N}} \stackrel{\mathrm{def}}{=} \mathrm{diag}(d_1, \ldots, d_{\mathrm{N}}) \tag{5}$$

Next, the *volume* $\mathcal{V}$ and the *normalized Laplacian* $\mathcal{L}$ of the graph G is defined as

$$\upsilon(G) \stackrel{\mathrm{def}}{=} \sum_{i=1}^{i=N} d_i = \mathrm{tr}(\mathcal{D}) \tag{6}$$

Downloaded From: https://manufacturingscience.asmedigitalcollection.asme.org/ on 11/24/2015 Terms of Use: http://www.asme.org/about-asme/terms-of-use

$$\mathcal{L}^{N\times N} \stackrel{\text{def}}{=} \mathcal{D}^{-\frac{1}{2}} \times (\mathcal{D} - \mathbf{S}) \times \mathcal{D}^{-\frac{1}{2}}$$
$$\text{where } \mathcal{D}^{-\frac{1}{2}} = \text{diag}\left(\frac{1}{\sqrt{d_1}}, \ldots, \frac{1}{\sqrt{d_N}}\right) \tag{7}$$

$\mathcal{L}$ is analogous to Kirchhoff matrix encountered in electrical networks [15] . Thereafter, the eigen spectrum of $\mathcal{L}$ is computed as

$$\mathcal{L}v = \lambda^* \mathbf{v} \tag{8}$$

Note that $\mathcal{L}$ is symmetric positive semi-definite, i.e., $\mathcal{L} \geq 0$, its eigenvalues (λ^*) are non-negative, and bounded between 0 and 2, i.e., $0 \leq \lambda_i \leq 2$. The smallest nonzero eigenvalue (λ_2) is termed the *Fiedler number* and the corresponding eigenvector ($\mathbf{v}_2$) as the *Fiedler vector* [15,16]. Barring pathological scenarios that rarely occur in practical circumstances, the Fiedler number is strictly bounded between 0 and 1, i.e., $0 < \lambda_2 < 1$ [15,16]. The graph *topological invariant* Fiedler number (λ_2) is used as a quantifier for $\mathcal{X}$. Further physical interpretations of the Fiedler number (λ_2) are explained in our recent publication [32,33].

The point cloud deviations $\mathcal{X}$ contain information from various aspects of the part, e.g., profile, line, and GD&T; consequently, the Fielder number (λ_2) is able to capture subtle aspects in the component dimensional integrity that are not discernable from statistical analysis and facet-based benchmarking alone. Essentially, the Fiedler number is a convolution of many aspects of dimensional integrity.

More pertinently, it is inferred that further the dimensions of a component deviate from the reference, the higher is the Fiedler number (λ_2). Hence, a comparatively larger Fielder number (λ_2) signifies parts with poor dimensional integrity. This will be demonstrated in Sec. 4 using experimental, as well as numerical, simulations. In Sec. 3.2.3, two different methods are described that are designed to accommodate the SGT approach in a practical scenario.

3.2.3 Methods for Practical Application of SGT. In this section, three different sampling schemas are developed for analyzing the 3D point cloud data $\mathcal{X}$. This is necessary for the following reasons: it is computationally intractable to obtain the Fiedler number over the complete part. For instance, given 3D point measurements ($\mathcal{X}$) over 500,000 spatial locations in Eq. (1), would entail 25×10^{10} pairwise comparisons to obtain $\mathbf{S}$ (Eqs. (2) and (3)). We will explore methods to make the approach computationally tractable using different techniques to sample the 3D point cloud data.

SGT-method 1: Random sampling of point cloud measurements. This method randomly samples the acquired 3D point cloud deviations $\mathcal{X}^{N\times d}$, where N is the number of data points and d is the number of dimensions (x, y, and z Cartesian coordinate axes), with contiguous, nonoverlapping windows. The method consists of the following steps:

- Step 1: From the point cloud sequence $\mathcal{X}^{N\times d}$ random sample m points without replacement, i.e., obtain $\mathscr{X}^{m\times d}$, $\mathscr{X} \subseteq \mathcal{X}$. Essentially, randomly pick m rows from the matrix $\mathcal{X}$. The sample size m is taken to be ~2/3rd of the total data size N. In this work, m translates to 300,000 data points.
- Step 2: Apply a windowing procedure (Fig. 6) to the subsample space $\mathscr{X}$, as follows. Split $\mathscr{X}^{m\times d}$ into n smaller matrices $\mathbf{X}_h^{k\times d}$, $h = \{1..n\}$, such that $k \times n = m$. The procedure is equivalent to operating a (nonoverlapping) sliding window of size k on a signal $\mathscr{X}$ along the time domain. In block matrix form, this can be written as

$$\mathscr{X}^{m\times d} = [[\mathbf{X}_1^{k\times d}], [\mathbf{X}_2^{k\times d}], \ldots [\mathbf{X}_m^{k\times d}]]_{m\times 1}{}^{\mathrm{T}} \tag{9}$$

The key challenge is to select a sufficiently large window size k, that does not impose computation constraints; unfortunately, this is a heuristic choice. Based on the trials, an appropriate value of k was observed to be in the vicinity of 0.05% to 0.1% of the length of total data N, which in our case is ~500,000 data points. Accordingly, k was set to 500 for all subsequent analysis.

- Step 3: Estimate the Fiedler number λ_2^{h} using Eqs. (2)–(8) for each subsample $\mathbf{X}_{\mathrm{h}}$ in Eq. (9). This step can be distilled as

$$\mathbf{\Lambda}_2 = [\,\lambda_2^1 \quad \lambda_2^2 \quad \cdots \quad \lambda_2^m\,]^{\mathrm{T}} \tag{10}$$

The key advantages of this method are that it is simple and eliminates inherent instrument and measurement bias, and is computationally efficient as it requires only a sample of the whole data. These steps are summarized in pseudocode form in Fig. 6. This windowing procedure is used again in Method 2.

SGT-method 2: Spatial localization of geometric deviation from point cloud measurements. The previous approach did not consider the spatial sequence of the data. Hence, it cannot be used for identifying the specific location of a defect on the component. In contrast, the present method preserves the spatial information by following these steps:

- Step 1: Sort the point cloud data deviations $\mathcal{X}^{N\times d}$ in either the x or y direction based on the corresponding reference coordinates $\mathcal{R}$. It is implicitly assumed that the material layers are deposited in the z direction. Let $\overline{\mathcal{X}}$ be the sorted point cloud deviations matrix. $\overline{\mathcal{X}}$ therefore preserves spatial information.
- Step 2: Split the sorted deviation matrix $\overline{\mathcal{X}}$ into n equal windows by applying the windowing procedure described in SGT-Method 1 (Fig. 6).

However, in this method, the windowing procedure is slightly modified. Instead of fixing the window size k as done in SGT-Method 1, in SGT-Method 2 the number of windows n is fixed and then we compute the window size k. This has the effect of slicing the component into n strips of identical width. An example of such spatial sampling is shown in Fig. 9(*a*). If n is set at 500, as is done for all instances in this work, then each sampling window is approximately 10 mils (0.010 in.) in width (250 μm), and 0.3 in. (8 mm) in height for the NIST sample (Fig. 3). Because of such spatial sampling, the sequence $\mathbf{\Lambda}_2(n) = [\,\lambda_2^1 \quad \lambda_2^2 \quad \cdots \quad \lambda_2^n\,]^{\mathrm{T}}$ is mapped to a particular area on the component. Consequently, it is possible to track which facet has deviated relative to the design blueprint dimensions.

4 Discussion of Results

The SGT approach is now applied, first to the experimentally acquired point cloud data (Sec. 4.1), followed by analysis of artificially generated samples (Sec. 4.2). These numerical studies augment the experimental results by seeking to quantify the change in Fiedler number with controlled variation in dimensional integrity. Computer generated case studies are necessary for this purpose because, from a practical standpoint, dimensional integrity is not a precisely controllable set point.

4.1 Application to AM Surfaces. Results from application of the SGT approach to experimental 3D point cloud data using the two different sampling methods discussed in Sec. 3.2.3 are shown in Fig. 7 and Table 3. The following inferences are made based on these results:

(1) **Referring to Figs. 7(*a*1) and 7(*b*1)**, which shows the mean Fiedler number (λ_2) (from the Fiedler number sequence $\mathbf{\Lambda}_2$) for different test parts obtained using the two SGT-methods developed in Sec. 3.2.3, the Fiedler number (λ_2) demonstrates a consistent trend, namely, λ_2 (CF-ABS platform) $< \lambda_2$ (ABS chamber) $< \lambda_2$ (ABS platform). This trend is unambiguous regardless of the sampling method applied. The error bars in Figs. 7(*a*1) and 7(*b*1) indicate a

Downloaded From: https://manufacturingscience.asmedigitalcollection.asme.org/ on 11/24/2015 Terms of Use: http://www.asme.org/about-asme/terms-of-use

```
procedure windowing(x^{m×d}, k)   // k is length of window, e.g. k = 500
n = ⌊m/k⌋;                        // n is number of windows, m is the sample size
w = k;
i = 1;
    For (h =1; h ≤ n; h++)
        Compute λ_2^h;                                   (Eqns. (2)- (8))
        X_h^{k×d} = X^{N×d}(i:w, 1:d);                   (Eqn. (9))
        i = 1 + w;
        w = k + w;
    end
Return Λ_2 = [λ_2^1  λ_2^2  ⋯  λ_2^n]^T;                 (Eqn. (10))
```

Fig. 6 Pseudocode for the windowing procedure

two-sided 95% confidence interval (CI) on the mean Fiedler number (λ_2). In contrast, the benchmark methods one (statistical feature mining, Fig. 4) and two (facet examination, Fig. 5) techniques were not able to reliably capture differences between the test parts.

(2) **Referring to Table 3**, which presents results from statistical analysis of the SGT method, such as CIs and ANOVA, it is observed that the difference in Fiedler number across different test components is statistically significant (p-value $<1\%$) irrespective of the sampling method used for estimation. Tukey's comparison test revealed that the pairwise difference in Fiedler number for the various test components is also statistically significant (p-value $<1\%$); the statistical significance was $<1\%$ for all pairwise comparisons between test components. Therefore, it can be statistically confirmed that λ_2 (CF-ABS platform) $<\lambda_2$ (ABS chamber) $<\lambda_2$ (ABS platform) with 99% confidence.

(3) In light of the foregoing observations (1) and (2), the dimensional integrity of the test components can be classified quantitatively in the following order: CF-ABS platform

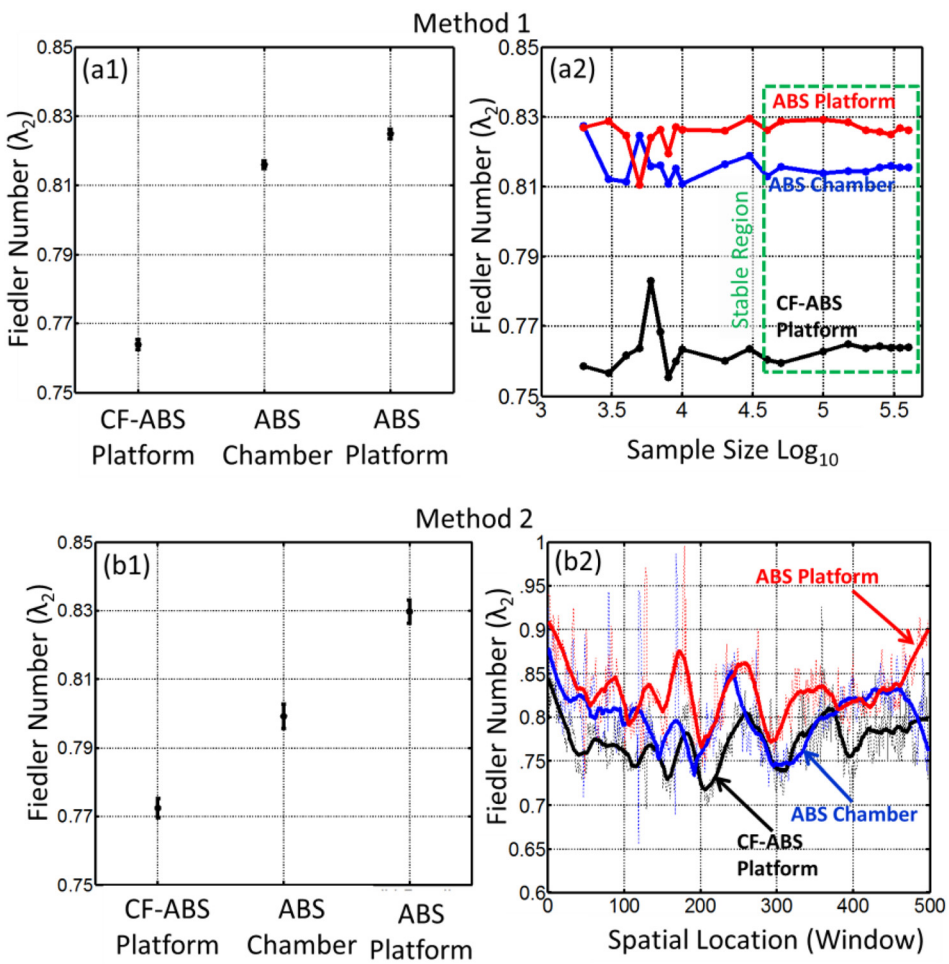

Fig. 7 Results from applying the SGT approach to experimental test components. (*a*1) and (*b*1) The Fiedler number for the three different components using two different sampling methods described in Sec. 3.2.3. The difference in Fiedler number across test components is statistically significant (p-value <0.01) The trends in Fiedler number are similar irrespective of the sampling method. The error bars represent the two-sided 95% CI on the mean. (*a*2): The Fiedler number vs. sample size (m) for Method 1. The Fiedler number converges for $m>50,000$. (*b*2): The Fiedler number vs. spatial location on component using Method 2 notice the generally smaller magnitude of the CF component.

Downloaded From: https://manufacturingscience.asmedigitalcollection.asme.org/ on 11/24/2015 Terms of Use: http://www.asme.org/about-asme/terms-of-use

(best adherence to specifications), ABS chamber (midway), ABS platform (worst dimensional integrity).

(4) **Referring to Fig. 7(*a*2)**, which depicts the mean of the Fiedler number sequence $\Lambda_2(m)$ for each of the three test components obtained from Method 1, Sec. 3.2.3. The 3D point cloud sample size is varied from $m = 2000$ to $m = 400,000$. For small samples sizes, $m < 10,000$, the Fiedler number has an ambiguous trend for the three test components. Nonetheless, the Fiedler number estimates begin to show a clearer demarcation for sample sizes beyond $m > 10,000$, converging to a stable value for $m > 50,000$ (the Fiedler number estimates for $m = 300,000$ is shown in Fig. 7(*a*1)). This result is in agreement with our previous inferences—the Fiedler number (λ_2) has a consistent trend, namely, λ_2 (CF-ABS platform) $< \lambda_2$ (ABS chamber) $< \lambda_2$ (ABS platform).

(5) **Referring to Fig. 7(*b*2)**, which shows the Fiedler number sequence $\Lambda_2(n) = [\lambda_2^1 \quad \lambda_2^2 \quad \cdots \quad \lambda_2^{n=500}]^T$ across $n = 500$ spatial locations of equal area sorted along the x direction as described in SGT-Method 2, Sec. 3.2.3. The bold lines in Fig. 7(*b*) are smoothed approximations of the sequence $\mathbf{\Lambda}_2(n)$ obtained using a Savitsky–Golay filter. This is done in order to eliminate transient outliers in the data. It is observed that the Fiedler number sequence $\mathbf{\Lambda}_2(n)$ for the three test components is significantly different. In general, the CF-ABS platform component has the least Fiedler number (λ_2), while the ABS platform component has the largest. From a physical perspective, this again confirms that the CF component (CF-ABS platform) adheres closest to the specified dimensions.

(6) **Referring to Fig. 7(*b*2)**, a more pertinent pattern is reported at the edges (of Fig. 7(*b*2)), where the Fiedler number tends to increase for all components, which indicates possible warping near the edges of the component, as oftentimes observed in polymer extrusion AM techniques. The trend is perceptibly most acute for the ABS platform component. This observation exemplifies the utility of SGT-Method 2 for localizing defects, which will be further investigated in Sec. 4.2.2 using numerically generated point cloud data.

These results are indicative of the effectiveness of the Fiedler number (λ_2) for tracking the dimensional integrity of AM components from 3D cloud data. In Sec. 4.2, we will use computer-simulated components, where the level of dimensional deviation and measurement errors are closely controlled, to further corroborate the effectiveness of the Fiedler number.

4.2 Verification With Numerically Generated Point Cloud Data. In this section, point cloud data of test components are simulated with varying levels of geometric integrity. In order to ensure that the test data are in close accordance with experimental results, the 3D point cloud deviations ($\mathcal{X}$) from the ABS chamber component are used as a baseline or seed for generating new samples, this resembles a statistical bootstrapping procedure. Two case studies based on such simulated data are described below.

- case 1: Components having Gaussian distributed isotropic manufacturing errors with different levels of geometric deviation (Σ) (Sec. 4.2.1)
- case 2: Components having Gaussian distributed manufacturing errors with different levels of geometric deviation (Σ) at specific locations of the component (Sec. 4.2.2)

4.2.1 Case 1: Components Having Gaussian Distributed Manufacturing Errors With Different Levels of Geometric Deviation (Σ). This study aims to quantify the sensitivity of the Fiedler number (λ_2) to variations in dimensional integrity of components. For this purpose, it is assumed that components are produced with varying levels of overall dimensional integrity; and that the geometric deviations are isotrpically/homogeneously distributed over the entirety of the component, as opposed to a specific location. In order to control the level of deviations from the normal process condition, new 3D point cloud data $\widetilde{\mathcal{X}}$ are randomly generated from the empirically obtained 3D point cloud $\mathcal{X}$ (from the ABS chamber component) in the following manner:

$$\widetilde{\mathcal{X}} = \begin{bmatrix} \mathbf{N}(x_1^1 + \sigma^1) & \cdots & \mathbf{N}(x_1^d + \sigma^d) \\ \vdots & \ddots & \vdots \\ \mathbf{N}(x_N^1 + \sigma^1) & \cdots & \mathbf{N}(x_N^d + \sigma^d) \end{bmatrix} \tag{11}$$

If one assumes $\sigma^1 = \sigma^2 = \cdots = \sigma^d = \Sigma$, then $\widetilde{\mathcal{X}} = \mathcal{X} + \mathbf{N}(0, \Sigma)$, where $\mathbf{N}$ is the matrix Gaussian distribution with mean 0 and standard deviation Σ. Essentially, for a point in $\mathcal{X}$, say $\boldsymbol{x}_i = \{x_i, y_i, z_i\}$, a new point is randomly sampled from a Gaussian distribution centered on $\boldsymbol{x}_i$ with standard deviation Σ. Physically, the parameter Σ represents the level of geometric deviations; $\Sigma = 0$ symbolizes the normal condition, i.e., original experimental point cloud data for the ABS chamber component.

The ABS chamber test part is implicitly assumed to be the normal condition, given that it is the seed data set $\mathcal{X}$ wherefrom $\widetilde{\mathcal{X}}$ is generated. No other statistical moments except the standard deviation are changed. Hence, all other the statistical moments, namely, mean, skewness, and kurtosis of the bootstrapped dataset $\widetilde{\mathcal{X}}$ will remain identical to $\mathcal{X}$. This assertion was verified using statistical tests (ANOVA).

As Σ increases, the generated point cloud deviations $\widetilde{\mathcal{X}}$ will veer farther away from $\mathcal{X}$. In other words, as Σ increases, the geometric integrity of the component worsens. Based on the physical insights [32,33] and previous empirical results (Sec. 4.1), a positive correlation is expected between Σ and Fiedler number (λ_2).

Table 3 Descriptive statistics and quantitative ANOVA results for the Fiedler number (λ_2) obtained using different methods. SSE: sum of squared errors; dfe: degrees of freedom for error; MSE: mean squared error; SST: treatment sum of squares; dft: treatment degrees of freedom; MST: mean of treatment sum of squares

Analysis Method →	SGT-Method 1			SGT-Method 2		
	$m = 300,000$; $k = 500$			$n = 500$		
Test component ↓	Mean λ_2	Std. error	± 95% CI on mean	Mean λ_2	Std. error	± 95% CI on mean
CF-ABS platform	0.7638	0.00077	0.0015	0.7724	0.0015	0.0029
ABS chamber	0.8160	0.00057	0.0011	0.7992	0.0018	0.0036
ABS platform	0.8250	0.00070	0.0014	0.8297	0.0017	0.0034
SSE/dfe = MSE		0.5123/1794 = 0.000285			2.1198/1491 = 0.0014	
SST/dft = MST		1.30353/2 = 0.6527			0.8186/2 = 0.4093	
Pooled Std. Dev		0.0169			0.0377	
F-statistic = MST/MSE		2285.5			287.89	
F-critical (0.95, dft, dfe)		3.0007			3.0018	
Tukey-pairwise distance		0.0023			0.0056	

Downloaded From: https://manufacturingscience.asmedigitalcollection.asme.org/ on 11/24/2015 Terms of Use: http://www.asme.org/about-asme/terms-of-use

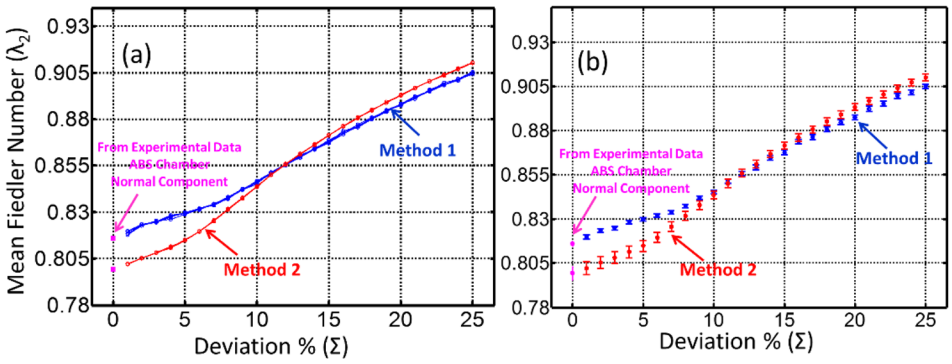

Fig. 8 Fiedler number obtained from the simulated point cloud data using SGT methods 1 and 2 at different levels of deviation (Σ). (*a*) Mean Fiedler number from five-fold cross validation (five replications). The difference between replications is statistically indistinguishable; the mean Fiedler numbers are estimated across replications after averaging over sample windows for a particular replication. (*b*) The Fiedler number shown along with the 95% CI interval for one particular replication. The mean Fiedler numbers are estimated across sample windows.

By generating 3D point cloud data with differing geometric deviations Σ; each Σ_u can be considered to represent a different process condition indexed by the integer u. Additionally, results are reported from a fivefold replication procedure, i.e., given a process condition t, there will be five repetitions of Σ: $\Sigma_t^1 \cdots \Sigma_t^5$, $t \in \{1 \ldots u\}$. Σ is a set based on the statistical standard deviation of the empirical 3D point cloud data $\mathcal{X}$. For instance, if the overall standard deviation of $\mathcal{X}$ is estimated to be $\sigma_{\mathcal{X}}$, then $\Sigma = \alpha\sigma_{\mathcal{X}}$, where $0 \leq \alpha$. For the ABS chamber component, $\sigma_{\mathcal{X}}$ was computationally estimated to be ~0.005 in. (~130 μm). In this study, Σ is varied from 1% to 25% of $\sigma_{\mathcal{X}}$; i.e., α is maintained in the range of $0.01 \leq \alpha \leq 0.25$. The results from the analysis are shown in Fig. 8.

The mean Fiedler number (λ_2) from the fivefold cross validation is shown in Fig. 8(*a*), whereas results from one particular replication are shown in Fig. 8(*b*) along with the 95% CI on the mean. The sampling/windowing parameters for each of the two methods are identical to those used for analyzing the experimental data (see Table 2). The window parameter (k) for SGT-Method 1 the sample size $m = 300{,}000$ and window length $k = 500$; and for SGT-Method 2 the number of partitions $n = 500$.

From Figs. 8(*a*) and 8(*b*), it is shown that the Fiedler number (λ_2) is positively correlated with deviation Σ. This confirms that the Fiedler number is related to the dimensional integrity of the component—the Fiedler number increases as the component dimensions deviate farther away from the nominal (which in our case is the ABS chamber test part). As before, SGT-Method 1 has the tighter CI bound on the mean Fiedler number (λ_2) compared with SGT-Method 2. This implies SGT-Method 1 could be the preferred approach for classification applications.

Continuing with the analysis, the Tukey's pairwise comparison test was conducted with these results. In general, the Fiedler number is statistically different (p-value <1%) for about 2% change in deviation (Σ). The result improves considerably if Method 1 is exclusively applied for classification purposes, in such a case a change in deviation as small as $\Sigma = 1\%$ can be captured. In contrast, statistical moments of the point cloud deviation $\tilde{\mathcal{X}}$, such as mean, skewness, kurtosis, in all of the three axis were not sensitive to change in Σ. This is to be expected, because the data was generated by keeping all other statistical moments constant except the standard deviation. In closing, it is noted that the ability of the SGT approach in detecting geometric deviations is physically constrained by the fidelity of the measurement. The FaroArm laser scanner used in this study has an accuracy of ± 43 μm.

4.2.2 Case 2: Spatial Localization of Anomalies. The aim of this study is to verify that the Fiedler number can indeed identify anomalous areas of an AM component. Whereas, in the previous case (Sec. 4.2.1), it had been assumed that the dimensions of the component vary homogenously throughout; in contrast, in this

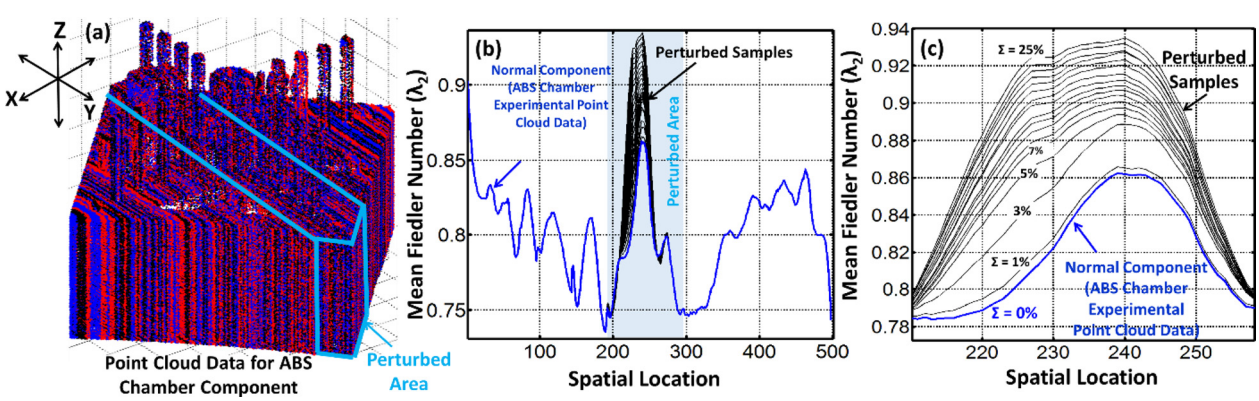

Fig. 9 Localizing component anomalies to specific areas using the Fiedler number. (*a*) The sorted point cloud data in *x*-direction. Each differently colored strip represents a sampling area or spatial location. There are 500 such location on the part, each containing approximately of 1000 data points, and measuring ~10 mils (250 μm) in width and ~0.3 in. (8 mm) in height. The portion marked in the middle is the location of interest in this case study, and is purposely perturbed. (*b*) The Fiedler number vs. the sampling location. The blue line is from the experimental ABS chamber part (Σ = 0, normal condition), a clear departure from the norm is observed as Σ increases. (*c*) Magnified view of the portion highlighted in (*b*).

Downloaded From: https://manufacturingscience.asmedigitalcollection.asme.org/ on 11/24/2015 Terms of Use: http://www.asme.org/about-asme/terms-of-use

study, location specific deviations will be deliberately created while the rest of the component remains unchanged.

For this purpose, the ABS chamber point cloud deviations $\mathcal{X}$ will be used, and subsequently, sorted along either the x or y directions, thus obtaining the sorted deviation matrix $\overline{\mathcal{X}}$ as done previously in Method 2, Sec. 3.2.3. However, instead of generating point cloud transformations uniformly for all locations as done in the previous case, only a specific area will be perturbed, in this case the middle portion highlighted in Fig. 9(*a*).

Each differently colored strip in Fig. 9(*a*) represents a spatial sampling window from the sorted point cloud matrix $\overline{\mathcal{X}}$. There are 500 such sampling windows or locations on the component ($n = 500$), each containing close to 1000 data points. Each sampling window physically measures 10 mils in width (250 μm, x-axis), and ~0.3 (8 mm, z-axis) inch in height. The point cloud data only in the middle 20% (amounting to about 100 windows, or ~100,000 data points, 25 mm) of the component corresponding to the marked strip in Fig. 9(*a*) will be perturbed under different levels of Σ in this study. Again, α is maintained in the range $0.01 \leq \alpha \leq 0.25$.

The point cloud data is analyzed as suggested in SGT-Method 3, Sec. 3.2.3. The Fiedler number sequence $\Lambda_2(n)$ for each spatial location is shown in Fig. 9(*b*). The highlighted portion of Fig. 9(*b*) corresponds to the perturbed area in Fig. 9(*a*); Fig. 9(*c*) is a magnified view of this perturbed area. From Figs. 9(*b*) and 9(*c*), it is observed that the Fiedler number identifies location specific deviations. As the dimensional integrity of a specific portion of the component worsens (Σ increases), the Fiedler number (λ_2) for that portion also increases, as seen in Fig. 9(*c*). Consequently, there will be a marked departure in the Fiedler number sequence $\Lambda_2(n)$ corresponding to the anomalous area of the workpiece.

For instance, the blue line in Figs. 9(*b*) and 9(*c*) is the Fiedler number sequence for the part with $\Sigma = 0$, which in our case is obtained from the experimental ABS chamber component (see also Fig. 7(*c*2)); the black lines correspond to different values of Σ (1–25%). Only half of the lines are shown in Fig. 9(*c*) for the sake of clarity. This result allows us to compare the measured trend against the baseline control ($\Sigma = 0$), and thus pinpoint the location, as well as magnitude of deviations from the nominal state.

5 Concluding Remarks and Future Work

A novel SGT approach for quantifying the dimensional integrity of complex geometry AM components has been developed and validated. Using the SGT-based topological quantifier, i.e., Fiedler number (λ_2), subtle variations in dimensional integrity for AM components fabricated under different test conditions can be effectively captured. Specific contributions from this work are as follows:

(1) The primary objective of this work was to quantify the geometric integrity of components fabricated with AM techniques. For illustrative purposes, three test components produced using different AM processes and/or materials were used in our comparison study. The SGT approach was able to succinctly classify the dimensional integrity of the test components in the following order: CF-ABS platform (best adherence to specifications), ABS chamber (midway), ABS platform (worst). This corresponds to ordering of the Fiedler number (λ_2), viz., λ_2 (CF-ABS platform) $< \lambda_2$ (ABS chamber) $< \lambda_2$ (ABS platform).

(2) Two different sampling methods were proposed in which the Fiedler number (λ_2) could be generated from point cloud data. The results were found to be consistent irrespective of the applied sampling methods, i.e., λ_2 (CF-ABS platform) $< \lambda_2$ (ABS chamber) $< \lambda_2$ (ABS platform).

(3) The proposed two SGT methods were verified by evaluating two case studies in which statistical variability was simulated by superimposing a certain amount of variation onto the scanned point cloud data. In the first case study, the statistical variation was gradually increased from its normal state, which amounted to a degradation in component dimensional integrity. The Fiedler number trends demonstrated an approximate positive correlation with statistical variation. This substantiates results from the experimentally acquired 3D point cloud data—the Fiedler number increases as dimensional integrity worsens.

(4) Furthermore, using SGT-Method 2, a spatial sampling approach, changes in dimensional integrity from its normal state corresponding to specific locations on the component can be isolated. This is advantageous from an application perspective, particularly for process diagnosis purposes. For instance, by identifying which locations on a component are consistently produced out of specification, a readjustment of process conditions or redesign of troublesome features can be considered.

The main shortcoming of the SGT approach is that the Fiedler number (λ_2) has not been correlated in this work with GD&T measurements. In the absence of such a correlation, it is not possible to infer the dimensional integrity of landmark features in terms of absolute GD&T measurements. Our future research objective is to relate the Fiedler number with specific GD&T measurements. Essentially, the proposed SGT method is a relative classifier of dimensional integrity of AM parts, i.e., akin to a differential comparator. In general, the proposed SGT method has been demonstrated to be an effective technique for characterizing the dimensional integrity of an AM component, which has been a long-standing and inherent problem for the AM community. This research therefore addresses the bourgeoning need in the AM community to address qualification and certification of complex components in future applications.

Acknowledgment

This research was sponsored by the following federal research Grant Nos.: National Science Foundation CMMI 1436592; and U.S. Department of Energy, Office of Energy Efficiency and Renewable Energy, Advanced Manufacturing Office, under Contract No. DE-AC05-00OR22725 with UT-Battelle, LLC. We thank the journal associate editor and the three anonymous reviewers for their helpful suggestions.

References

[1] Gibson, I., Rosen, D. W., and Stucker, B., 2010, *Additive Manufacturing Technologies: Rapid Prototyping to Direct Digital Manufacturing*, Springer, New York.

[2] Beyer, C., 2014, "Strategic Implications of Current Trends in Additive Manufacturing," ASME J. Manuf. Sci. Eng., **136**(6), p. 064701.

[3] NIST, 2013, "Measurement Science Roadmap for Metal-Based Additive Manufacturing," report prepared by Energetics Corporation, National Institute of Standards and Technology, Gaithersburg, MD, http://www.energetics.com/industrial-1/2015/2/10/measurement-science-roadmap-for-metal-based-additive-manufacturing

[4] Savio, E., De Chiffre, L., and Schmitt, R., 2007, "Metrology of Freeform Shaped Parts," CIRP Ann.–Manuf. Technol., **56**(2), pp. 810–835.

[5] Huang, Y., Leu, M. C., Mazumder, J., and Donmez, A., 2015, "Additive Manufacturing: Current State, Future Potential, Gaps and Needs, and Recommendations," ASME J. Manuf. Sci. Eng., **137**(1), p. 014001.

[6] Moylan, S., Cooke, A., Jurrens, K., Slotwinski, J., and Donmez, M. A., 2012, "A Review of Test Artifacts for Additive Manufacturing," National Institute of Standards and Technology (NIST), Gaithersburg, MD, Report No. NISTIR 7858.

[7] Love, L., Kunc, V., Rios, O., Duty, C., Elliot, A., Post, B., Smith, R., and Blue, C., 2014, "The Importance of Carbon Fiber to Polymer Additive Manufacturing," J. Mater. Res., **29**(17), pp. 1892–1898.

[8] Cooke, A., and Soons, J., "Variability in the Geometric Accuracy of Additively Manufactured Test Parts," 21st Annual International Solid Freeform Fabrication Symposium, Austin, TX, pp. 1–12.

[9] Atzeni, E., Iuliano, L., Minetola, P., and Salmi, A., 2012, "Proposal of an Innovative Benchmark for Accuracy Evaluation of Dental Crown Manufacturing," Comput. Biol. Med., **42**(5), pp. 548–555.

Downloaded From: https://manufacturingscience.asmedigitalcollection.asme.org/ on 11/24/2015 Terms of Use: http://www.asme.org/about-asme/terms-of-use

[10] Dimitrov, D., van Wijck, W., Schreve, K., and de Beer, N., 2006, "Investigating the Achievable Accuracy of Three Dimensional Printing," Rapid Prototyping J., **12**(1), pp. 42–52.
[11] Gervasi, V. R., Schneider, A., and Rocholl, J., 2005, "Geometry and Procedure for Benchmarking SFF and Hybrid Fabrication Process Resolution," Rapid Prototyping J., **11**(1), pp. 4–8.
[12] Ippolito, R., Iuliano, L., and Gatto, A., 1995, "Benchmarking of Rapid Prototyping Techniques in Terms of Dimensional Accuracy and Surface Finish," CIRP Ann.–Manuf. Technol., **44**(1), pp. 157–160.
[13] Mallepree, T., and Bergers, D., 2009, "Accuracy of Medical RP Models," Rapid Prototyping J., **15**(5), pp. 325–332.
[14] Rengier, F., Mehndiratta, A., von Tengg-Kobligk, H., Zechmann, C. M., Unterhinninghofen, R., Kauczor, H. U., and Giesel, F. L., 2010, "3D Printing Based on Imaging Data: Review of Medical Applications," Int. J. Comput. Assist. Radiol. Surg., **5**(4), pp. 335–341.
[15] Chung, F. R. K., 1997, *Spectral Graph Theory*, American Mathematical Society, Providence, RI.
[16] Fiedler, M., 1973, "Algebraic Connectivity of Graphs," Czech. Math. J., **23**(2), pp. 298–305.
[17] Mahesh, M., Wong, Y., Fuh, J., and Loh, H., 2004, "Benchmarking for Comparative Evaluation of RP Systems and Processes," Rapid Prototyping J., **10**(2), pp. 123–135.
[18] El-Katatny, I., Masood, S. H., and Morsi, Y. S., 2010, "Error Analysis of FDM Fabricated Medical Replicas," Rapid Prototyping J., **16**(1), pp. 36–43.
[19] Weheba, G., and Sanchez-Marsa, A., 2006, "Using Response Surface Methodology to Optimize the Stereolithography Process," Rapid Prototyping J., **12**(2), pp. 72–77.
[20] Arrieta, C., 2012, "Quantitative Assessments of Geometric Errors for Rapid Prototyping in Medical Applications," Rapid Prototyping J., **18**(6), pp. 431–442.
[21] Munguía, J., de Ciurana, J., and Riba, C., 2008, "Pursuing Successful Rapid Manufacturing: A Users' Best-Practices Approach," Rapid Prototyping J., **14**(3), pp. 173–179.
[22] Paul, R., Anand, S., and Gerner, F., 2014, "Effect of Thermal Deformation on Part Errors in Metal Powder Based Additive Manufacturing Processes," ASME J. Manuf. Sci. Eng., **136**(3), p. 031009.
[23] Siraskar, N., Paul, R., and Anand, S., 2015, "Adaptive Slicing in Additive Manufacturing Process Using a Modified Boundary Octree Data Structure," ASME J. Manuf. Sci. Eng., **137**(1), p. 011007.
[24] Nelaturi, S., Kim, W., and Kurtoglu, T., 2015, "Manufacturability Feedback and Model Correction for Additive Manufacturing," ASME J. Manuf. Sci. Eng., **137**(2), p. 021015.
[25] Pal, D., Patil, N., Zeng, K., and Stucker, B., 2014, "An Integrated Approach to Additive Manufacturing Simulations Using Physics Based, Coupled Multiscale Process Modeling," ASME J. Manuf. Sci. Eng., **136**(6), p. 061022.
[26] Kruth, J. P., Bartscher, M., Carmignato, S., Schmitt, R., De Chiffre, L., and Weckenmann, A., 2011, "Computed Tomography for Dimensional Metrology," CIRP Ann.–Manuf. Technol., **60**(2), pp. 821–842.
[27] Jiang, X., Scott, P., and Whitehouse, D., 2007, "Freeform Surface Characterisation–A Fresh Strategy," CIRP Ann.–Manuf. Technol., **56**(1), pp. 553–556.
[28] Bi, Z. M., and Wang, L., 2010, "Advances in 3D Data Acquisition and Processing for Industrial Applications," Rob. Comput. Integr. Manuf., **26**(5), pp. 403–413.
[29] Tang, P., Huber, D., Akinci, B., Lipman, R., and Lytle, A., 2010, "Automatic Reconstruction of As-Built Building Information Models From Laser-Scanned Point Clouds: A Review of Related Techniques," Autom. Constr., **19**(7), pp. 829–843.
[30] Raja, V., Zhang, S., Garside, J., Ryall, C., and Wimpenny, D., 2005, "Rapid and Cost-Effective Manufacturing of High-Integrity Aerospace Components," Int. J. Adv. Manuf. Technol., **27**(7–8), pp. 759–773.
[31] El-Katatny, I., Masood, S., and Morsi, Y., 2010, "Error Analysis of FDM Fabricated Medical Replicas," Rapid Prototyping J., **16**(1), pp. 36–43.
[32] Rao, P. K., 2013, "Sensor-Based Monitoring and Inspection of Surface Morphology in Ultraprecision Manufacturing Processes," Ph.D. thesis, Oklahoma State University, Stillwater, OK.
[33] Rao, P. K., Beyca, O. F., Kong, Z., Bukkaptanam, S. T., Case, K. E., and Komanduri, R., 2015, "A Graph Theoretic Approach for Quantification of Surface Morphology and Its Application to Chemical Mechanical Planarization (CMP) Process," IIE Trans., **47**(10), pp. 1088–1111.

Downloaded From: https://manufacturingscience.asmedigitalcollection.asme.org/ on 11/24/2015 Terms of Use: http://www.asme.org/about-asme/terms-of-use